THE JOURNAL OF BIOLOGICAL CHEMISTRY VOL. 286, NO. 4, pp. 2998–3006, January 28, 2011

Possible Roles of Exceptionally Conserved Residues around the Selectivity Filters of Sodium and Calcium Channels*[S]

Received for publication, August 14, 2010, and in revised form, November 14, 2010 Published, JBC Papers in Press, November 16, 2010, DOI 10.1074/jbc.M110.175406

Denis B. Tikhonov[‡§] **and Boris S. Zhorov**[‡§1]

From the [‡]*Department of Biochemistry and Biomedical Sciences, McMaster University, Hamilton, Ontario L8N 325, Canada and the* [§]*Sechenov Institute of Evolutionary Physiology and Biochemistry, Russian Academy of Sciences, St. Petersburg 194 223, Russia*

In the absence of x-ray structures of sodium and calcium channels their homology models are used to rationalize experimental data and design new experiments. A challenge is to model the outer-pore region that folds differently from potassium channels. Here we report a new model of the outer-pore region of the NaV1.4 channel, which suggests roles of highly conserved residues around the selectivity filter. The model takes from our previous study (Tikhonov, D. B., and Zhorov, B. S. (2005) *Biophys. J.* 88, 184–197) the general disposition of the P-helices, selectivity filter residues, and the outer carboxylates, but proposes new intra- and inter-domain contacts that support structural stability of the outer pore. Glycine residues downstream from the selectivity filter are proposed to participate in knob-into-hole contacts with the P-helices and S6s. These contacts explain the adapted tetrodotoxin resistance of snakes that feed on toxic prey through valine substitution of isoleucine in the P-helix of repeat IV. Polar residues five positions upstream from the selectivity filter residues form H-bonds with the ascending-limb backbones. Exceptionally conserved tryptophans are engaged in inter-repeat H-bonds to form a ring whose π-electrons would facilitate passage of ions from the outer carboxylates to the selectivity filter. The outer-pore model of CaV1.2 derived from the NaV1.4 model is also stabilized by the ring of exceptionally conservative tryptophans and H-bonds between the P-helices and ascending limbs. In this model, the exceptionally conserved aspartate downstream from the selectivity-filter glutamate in repeat II facilitates passage of calcium ions to the selectivity-filter ring through the tryptophan ring. Available experimental data are discussed in view of the models.

Voltage-gated ion channels are involved in the control of many physiological functions. Upon membrane depolarization, channels rapidly transit from the resting to the open state, then close to inactivated state(s), and return to the resting state upon membrane repolarization. The human genome encodes nine voltage-gated sodium (NaV1.1-NaV1.9) and ten voltage-gated calcium channels categorized as L (CaV1.1-CaV1.4), P/Q (CaV2.1), N (CaV2.2), R (CaV2.3), and T (CaV3.1-CaV3.3) types. The pore-forming α_1-subunit of calcium and sodium channels folds from a single polypeptide chain of four homologous repeats (Fig. 1*A*). Repeats I to IV are arranged clockwise when viewed extracellularly (1). Each repeat contains a voltage-sensing domain S1-S4, an outer helix S5, an inner helix S6, and a membrane-diving P-loop between S5 and S6. The P-loop includes a P-helix, a P-turn, and an ascending limb. Four ascending limbs, which line the outer pore, contain selectivity-filter residues in positions *p50* (see Footnote 2 for residue labels).[2] Repeats I, II, III, and IV contain selectivity-filter glutamates in calcium channels (the EEEE ring) and Asp, Glu, Lys, and Ala residues in sodium channels (the DEKA ring). The ascending limbs also contain the outer carboxylates three or four positions downstream from the selectivity-filter residues.

Voltage-gated potassium, sodium, and calcium channels are believed to share a generally similar folding of transmembrane helices and P-helices (2, 3). This justifies homology modeling of sodium and calcium channels based on available x-ray structures of potassium channels. The homology models are used to predict structural peculiarities of sodium and calcium channels, propose mechanisms of ion permeation, and explain data on ligand actions. The most difficult region for homology modeling is the outer pore, whose folding in sodium and calcium channels is different from that in potassium channels.

Tetrodotoxin (TTX)[3] and saxitoxin, the hallmark outer-pore blockers of NaV1.4, were used to probe the outer-pore region. These data have been accommodated in competing models of NaV1.4 with the toxins (4, 5). Despite the fact that similar experimental data sets underlie the models, they differ significantly in terms of mutual disposition and orientation of the pore helices and conformations of the ascending limbs. An explanation for this difference is flexibility of side chains in the ascending limbs that according to experimental data interact with specific toxin moieties. This flexibility can compensate a substantial backbone difference between the two

* This study was supported by grants from Natural Sciences and Engineering Research Council of Canada, the Canadian Institutes of Health Research (MOP-53229) (to B. S. Z.), and by a grant from the RAS Program Molecular and Cell Biology (to D. B. T.).

[S] The on-line version of this article (available at http://www.jbc.org) contains supplemental Figs. S1 and S2.

[1] To whom correspondence should be addressed. Tel.: 905-525-9140 × 22049; Fax: 905-522-9033; E-mail: zhorov@mcmaster.ca.

[2] We designate residues using labels that are universal for P-loop channels (Fig. 1). A residue label includes repeat number, which is omitted if all repeats are referred to, segment index (*i*, **i**nner helix; *p*, **P**-loop; *o*, **o**uter helix), and position in the segment.

[3] The abbreviations used are: TTX, tetrodotoxin; DEKA, selectivity-filter ring of Asp, Glu, Lys, and Ala residues from the four P-loop domains of sodium channels; EEEE, selectivity-filter ring of glutamate residues from the four P-loop domains of calcium channels; MC, Monte Carlo; MCM, Monte Carlo minimization.

models. Thus, the toxin-channel distance constraints, which are derived from experiments, are insufficient for elaboration of an unambiguous model of the outer pore.

In previous models, the P-loop domains of sodium and calcium channels (4–7) had been built without serious considerations of the outer-pore stability. This stability can be supported by specific inter- and intra-repeat contacts including the ascending limbs that line the outer pore. The contacts, which stabilize the outer pore of potassium channels, are known from the crystallographic data. In sodium and calcium channels such contacts are unknown.

Multiple-sequence alignment of 137 voltage-gated calcium channel proteins shows exceptionally conserved residues in the P-domains, including the signature-sequence T*X*E*X*W with the selectivity filter glutamates (8). In the last decade, hundreds of new sequences of sodium and calcium channel proteins in various organisms have become available. Because the pore-forming α_1-subunits of voltage-gated calcium and sodium channels contain four homologous repeats, local sequence alignments of segments from individual repeats can be used to reveal conserved residues in each repeat. Considering highly conserved residues beyond the selectivity filter and their interaction patterns in homology models may suggest functional roles for these residues and new inter-residue interactions. These can be used as distance constraints to improve the homology models.

In this work we have generated and explored multiple sequence alignments of P-loops in individual repeats of hundreds of calcium and sodium channel proteins. Analysis of these alignments allowed us to propose a network of hydrophobic, hydrogen bonding, and knob-into-the-hole contacts involving conserved residues, which stabilize the outer-pore region. Using available experimental data and the above contacts as distance constraints, we elaborated our homology models (5, 6, 9). The new inter-repeat contacts suggest new important roles for some of the exceptionally conserved residues. The new models allow us to propose details of the ion permeation mechanisms in sodium and calcium channels and provide structural rationale for recent experimental data on sequence peculiarities of sodium channels in garter snakes that feed on toxic pray.

MATERIALS AND METHODS

To reveal conserved residues in the P-loops of sodium and calcium channels we aligned many sequences from the translated nucleotide database using NCBI BLAST program *tblastn*. Sequences of 21-amino acid segments, which include P-helices, P-turns, and ascending limbs in four repeats of NaV1.4 (SCN4A_HUMAN) and four repeats of CaV1.2 (CAC1C_HUMAN) were used as queries. Default parameters were used for the *tblasn* algorithm, except for the maximal number of aligned sequences, which was set to 5,000. The search was limited by the ENTREZ queries ("calcium channel" OR "Ca^{2+} channel") and ("sodium channel" OR "Na^{+} channel"). A total of ~6,000 sequences were returned. The sequence alignments for 21-amino acid segments of Ca^{2+} and Na^{+} channels returned by *tblastn* were unambiguous. To minimize the influence of possible errors in the data base, repeat entries that contained atypical residue types (less than four occurrences in a matching position) were excluded (8); about 3% of the sequences were thus excluded. We also manually removed sequences with insertions/deletions at the N or C termini. Unequal numbers of sequences returned for individual repeats may be due to the fact that most calcium and sodium channels are hetero-tetramers and in some cases sequences of specific repeats, which are too different from the query sequence, were not returned by *tblastn*. Detailed analysis of this possibility, which would require specific bioinformatics tools, is beyond the scope of this study.

The returned sequences were analyzed and manually condensed in Fig. 1 where different colors encode different levels of conservation. For some positions, we use Greek letters to encode residues with similar physico-chemical properties (see legend to Fig. 1). An amino acid may be attributed to different categories. For example, when leucine and methionine align in a matching position with other hydrophobic residues, we categorize all residues in this position as hydrophobic. However, when most of the residues in a matching position are leucine or methionine, we categorize them as long hydrophobic residues. Such categorization highlights conserved structural features (aromaticity, charge, length, β-branched atom), which will be useful for future elaboration of the models.

Homology models of NaV1.4 and CaV1.2 channels were built from the P-loop and S6 segments using the sequence alignments with potassium channels proposed before (7). The backbones of the ascending limbs were initially folded as in Ref. 5, 6. All calculations were performed using the ZMM program. The nonbonded energy was calculated using the AMBER force field (10, 11) with a cut-off distance of 8 Å. The hydration energy was calculated using the implicit solvent method (12). Electrostatic interactions were calculated using the distance-dependent dielectric function. The atomic charges of TTX have been calculated by the semi-empirical method AM1 (13) using MOPAC. The Monte Carlo-minimization method (14) was used to optimize the models. During energy minimizations, α carbons of the P-helices were constrained to their corresponding positions in the template using pins. A pin is a flat-bottom energy function, which allows an atom to deviate penalty-free up to 1 Å from the template and imposes a penalty of 10 kcal mol-1 Å-1 for deviations >1 Å.

Each model was MC-minimized until 2,000 consecutive minimizations did not decrease the energy of the apparent global minimum. The multi-MCM protocol (9) was used to dock TTX and impose specific distance constraints. No specific energy terms were used for cation-π interactions, which were accounted for due to partial negative charges at the aromatic carbons (15). Further details of methodology can be found elsewhere (9).

RESULTS

Analysis of Multiple Sequence Alignments—The multiple sequence alignments are summarized in Fig. 1*B* where residues are colored according to their conservation in individual repeats. As expected, most of the selectivity filter residues in positions *p50* (the DEKA ring in sodium channels and EEEE

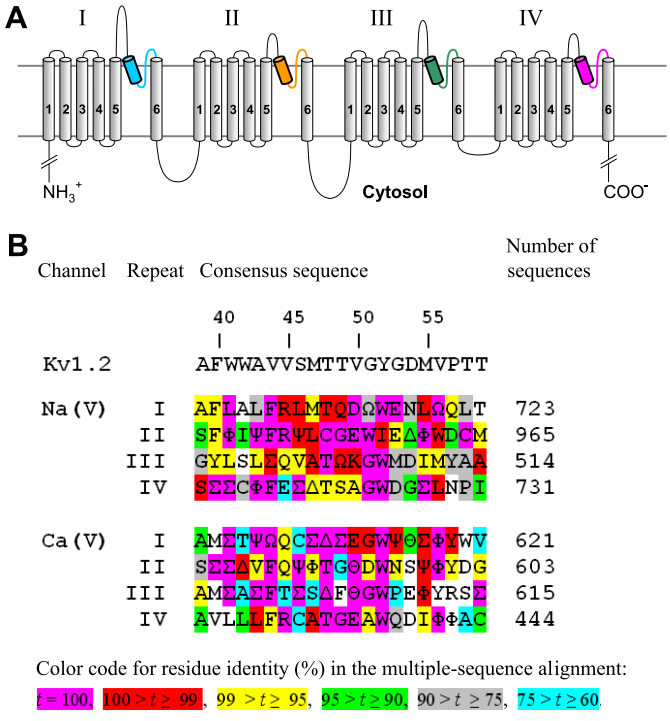

FIGURE 1. *A*, transmembrane topology of the pore-forming α_1-subunit in calcium and sodium channels. The α_1 subunit has four repeats. Each repeat contains six transmembrane helices (S1-S6), and a P-loop between S5 and S6 helices. The homology models in this study are composed of highlighted P-helices and ascending limbs, which contribute to the P-loops. P-helices and ascending limbs are colored as in the NaV1.4 models (Figs. 2–5). *B*, residue conservation in P-loops of sodium and calcium channels. Each position shows the dominant residue in the multiple sequence alignments obtained with query sequences CAC1C_Human (CaV1.2) and SCN4A_HUMAN (NaV1.4) for sodium and calcium channels, respectively. Greek letters encode residues of similar physico-chemical properties: Θ = E/D (acidic), Ω = Y/F (aromatic), Ψ = V/I (β-branched, hydrophobic), Φ = M/L (long hydrophobic), Σ = V/I/L/M/F (hydrophobic), Δ = S/T (hydroxy-substituted C^{β}). The *rightmost column* shows number of aligned sequences from the translated nucleotide database (nucleotide collection) found by *tblasn* with the respective query sequence. Relative numbers of residues in P-loops (3) are shown above the Kv1.2 sequence.

ring in calcium channels) are exceptionally (100%) conserved. The selectivity-filter alanine A^{4p50} in the sodium channels is highly (97.8%) conserved, and 2.2% of the sequences contain G^{4p50} or S^{4p50} residues. Also expected was a high conservation of the outer-carboxylate residues in the sodium channels. Thus, repeats I and II contain exceptionally conserved E^{1p53} and highly (99.0%) conserved E^{2p53} (Q^{2p53} in 1% of the sequences). Residues D^{3p54}, E^{3p54}, and Q^{3p54} are found respectively, in 71.2, 12.8, and 9.9% of repeat III sequences. Residues D^{4p53} and N^{4p53} are found, respectively, in 83.6 and 11.6% of repeat IV sequences (the remaining 4.8% of residues in this position are designated "B", *i.e.* either D or N). Three outer-carboxylates in positions *p53* are the TTX-sensing residues that were proposed to face the outer pore and interact with the TTX molecule (4, 5). In contrast, carboxylate *3p54* contributes to binding of μ-conotoxin (1) suggesting that it faces the extracellular media. In calcium channels the outer carboxylates in positions *1p54*, *3p54*, and *4p54* are moderately conserved suggesting that they are not critical for calcium permeation. A notable exception is a highly conserved D^{2p51} next to the selectivity filter glutamate E^{2p50}. Residue D^{2p51} was proposed by us to play an important role in calcium permeation (6).

The ascending limbs contain tryptophan residues, which are exceptionally conserved in all repeats of calcium and sodium channels. In all four repeats of calcium channels, these tryptophans are in the matching positions *p52*. Repeats I, III, and IV of Na^+ channels have tryptophans in position *p52*, whereas repeat II contains tryptophan W^{2p51}. Noteworthy, the matching position in calcium channels contains either highly conserved aspartate D^{2p51} (98%) or asparagine (2%). Sodium channels evolved from calcium channels (16). The exceptional conservation of the tryptophans and replacement of the calcium channel D^{2p51} with sodium channel W^{2p51} strongly suggests that these residues are important for key channel function(s). These are likely ion permeation and/or the outer-pore folding and stability.

Main peculiarities of the tryptophan side chain are the large planar heterocyclic ring with π-electrons, which may be engaged in π-cation interactions with permeating ions, and the NH group. Besides, the tryptophan side chain has the largest nonpolar surface area among naturally occurring amino acids. Examples of structural roles of tryptophans in proteins are shown in supplemental Fig. S1. In potassium channels the conserved tryptophans in the pore helix (positions *p41* and *p42*) participate in intra- and inter-subunit H-bonds, providing stabilization for the outer-pore structure (supplemental Fig. S1*A*). In some proteins, tryptophans form box-like structures, which accommodate cationic ligands (supplemental Fig. S1, *B* and *C*) with π-cations apparently contributing to the ligand-protein interactions.

Conserved Tryptophans in the Outer Pore of Sodium Channels—The high conservation of tryptophans in the ascending limbs of sodium and calcium channels has long been known (8) and all these tryptophans have been previously mutated in sodium channels. Cysteine substitutes of the ascending-limb tryptophans are accessible by externally applied methane thiosulfonate reagents (17). Furthermore, cysteine substitutions of W^{4p52}, W^{3p52}, and W^{1p51} form disulfide bonds involving engineered cysteines in the neighboring ascending limbs (18). These data strongly indicate that the side chains of the conserved tryptophans are not buried in the protein, but face the outer pore. Alanine substitutions of W^{4p52} alter the ionic selectivity of sodium channels (19). Cysteine substitution of W^{4p52} abolishes the NaV1.4 block by lidocaine (20), a local anesthetic that binds in the inner pore (15). W^{4p52} was suggested to directly interact with the local anesthetic bound in the inner pore (20), but in view of our models of sodium channels, direct contact of W^{4p52} with the local anesthetic molecule is unlikely, suggesting that the mutation $W^{4p52}C$ affects the drug binding allosterically. W^{1p51} was proposed to contribute to the pore of the sodium channel (21).

Even though the above studies imply importance of the outer-pore tryptophans, their structural and functional roles, which underlie the exceptional conservation, remain unclear. How could one arrange the pore-facing side chains of the conserved tryptophans? The tryptophans are unlikely to face the pore lumen with their edges because the side-chain NH

group and aromatic hydrogens would retard the cation permeation. The more likely possibility is that the tryptophans face the pore by their π-electron rich aromatic faces that would favorably interact with the permeating cations. Box-like structures involving tryptophans are seen in some proteins (supplemental Fig. S1, *B* and *C*). With this hypothesis in mind, we revised our previous model (5). In the previous model, the side chain of W^{3p52} is partially exposed to the pore and its NH hydrogen is 2.5–2.8 Å away from the backbone oxygen of W^{4p52}. This distance is ~1 Å larger than a typical H-bond length. Here we hypothesized that the side chain NH groups of the conserved tryptophans are engaged in inter-repeat H-bonds that stabilize the outer-pore structure. We biased the inter-repeat H-bond for W^{4p52} with a distance constraint and used analogous constraints to impose inter-repeat H-bonds involving the side chains of W^{1p52} and W^{4p52}. The side chain of W^{2p51} projects toward repeat I rather than to repeat III. Therefore, we imposed an H-bond between the side chain NH group of W^{2p51} and the backbone carbonyl of Y^{1p51}. We have used our previous model (5) as the starting structure, MC-minimized the model with the above constraints, and then refined it by unconstrained MC-minimizations. The proposed set of H-bonds was readily formed with only modest deformations of the ascending-limb backbones in the starting model (5).

The critical test for the new model was to explore whether the inter-repeat H-bonds agree with experimental data on TTX binding. Therefore, we energy-optimized the model with the TTX molecule bound to the outer pore as described before (5). To minimize distortions of the TTX receptor upon the ascending-limb deformations caused by new inter-repeat constraints, we used distance constraint to keep specific TTX interactions with the DEKA ring and the outer carboxylates as described before (5). More recent experimental data show that the aromatic ring of Y^{1p51} is engaged in π-cation interactions with TTX, which stabilize TTX binding in TTX-sensitive sodium channels (22). This non-conservative aromatic residue is a well-known determinant of TTX sensitivity (23–25). For example, NaV1.2 and NaV1.4, which have, respectively, F^{1p51} and Y^{1p51}, are TTX-sensitive, whereas the NaV1.5 channel, which has C^{1p51}, is low-sensitive to TTX. In our previous model Y^{1p51} faces the pore and approaches the TTX molecule, but it is not engaged in π-cation interaction with TTX (5). To satisfy the new experimental data (22), we imposed a distance constraint between the guanidinium group of TTX and the aromatic ring of Y^{1p51}. In the MC-minimized model, TTX fits perfectly in the outer pore, which is lined by tryptophans in positions *p52*, the highly conserved I^{2p52}, and a hydrophobically conserved residue in position *3p53* (Fig. 2). The outer carboxylate side chains E^{1p53}, E^{2p53}, and D^{4p53} protruded through the gaps between the tryptophans to make specific contacts with the TTX molecule (Fig. 2*A*) whose guanidinium group reached the selectivity-filter residues D^{1p50} and E^{2p50} (Fig. 2*B*) and was also engaged in cation-π interaction with Y^{1p51} (Fig. 2*C*). The position and orientation of the TTX molecule did not change substantially *versus* our previous model (5), while the ascending-limb backbones underwent only moderate changes. The TTX binding appeared invariant to these changes because TTX interacted with flexible side chains.

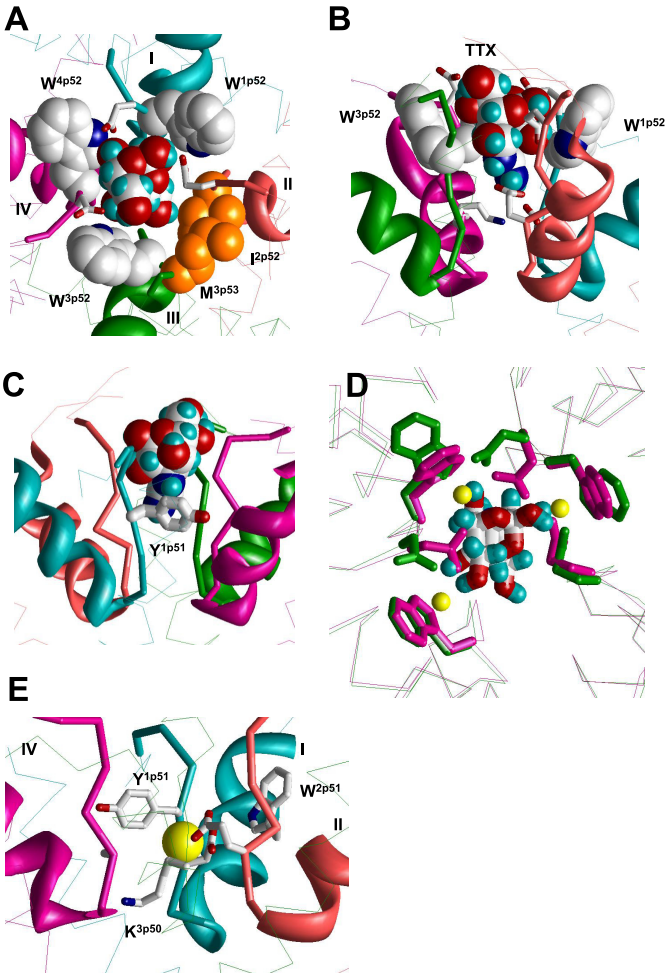

FIGURE 2. **Binding of TTX and Ca^{2+} in the revised model of NaV1.4.** *A* and *B*, top and side views of TTX-bound channel. Backbones in repeats I, II, III, and IV are *cyan*, *opaque*, *green*, and *magenta*, respectively. P-helices are shown as *ribbons*, ascending limbs as *thick* α-*tracings*, and S6s as *thin* α-*tracings*. TTX fits perfectly in the outer pore and interacts with known TTX-sensing residues. *C*, cation-π interaction between Y^{1p51} and guanidine group of TTX (22). This interaction is achieved by only a modest deformation of our previous model (5), in which Y^{1p51} faces the pore and interacts with TTX by the aromatic ring edge rather than the aromatic plane. *D*, superposition of α tracings of the current model, which is MC-minimized either in the presence of Na^+ ions (*yellow* Na^+ ions, *magenta* side chains and backbones) or TTX (*green* side chains and backbones). Side chains of W^{1p52}, W^{3p52}, W^{4p52}, and TTX-sensing outer carboxylates E^{1p53}, E^{2p53}, and D^{4p53} are shown as *sticks*. The root mean square deviation between α carbons in these models is as small as 0.2 Å. Note that hydroxyl groups of the TTX molecule are very close to positions of Na^+ ions. *E*, possible binding of a Ca^{2+} ion in the Na^+ channel. The ion binds to acidic residues D^{1p50} and E^{2p50} of the DEKA locus and displaces the ammonium group of K^{3p50} toward the inner pore. The aromatic side chains of Y^{1p51} and W^{2p51} are close enough to the Ca^{2+} ion to interact with it through water molecules in the first hydration shell. The complex likely corresponds to the blocked channel state. In the absence of another cation-binding site in the narrowest part of the outer pore, an incoming ion cannot displace the bound Ca^{2+} ion.

TTX-sensing Residues in the Pore Helices—Aside from well-known TTX-sensing residues in the ascending limbs, mutations of several other residues affect TTX binding. Intriguing examples are provided by the analysis of NaV1.4 sequences from garter snakes that feed on the tetrodotoxic newt (26). The single mutation $I^{4p46}V$ increases TTX resistance of the Warrenton population of garter snakes by more than 4-fold

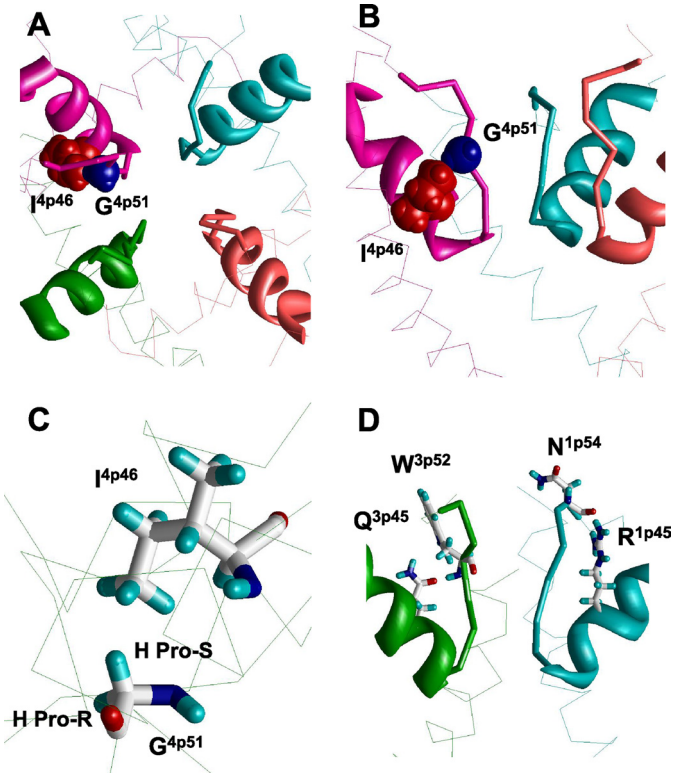

FIGURE 3. **Contacts between P-helices and ascending limbs contribute to the outer- pore stability.** *A* and *B*, top and side views at the outer pore of NaV1.4 in which space-filled G^{4p51} and I^{4p46} form a tight knob-into-the-hole contact in our model. Mutation $I^{4p46}V$ reduces TTX sensitivity of garter snakes that adapted to the tetrodotoxic newt pray (26). It is hardly possible to explain this fact by direct interaction of I^{4p46} with TTX. In view of our model, the $I^{4p46}V$ mutation would result in a deformation of the outer pore due to shift of G^{4p51}, which would move toward V^{4p46} to retain the knob-into-the-hole contact. This shift would move the ascending limb in domain IV. The ascending limb accommodates a TTX-sensing residue D^{4p53}, which would move away from the pore axis thus decreasing the TTX sensitivity. A native knob-into-the-hole contact in repeat III involves G^{3p51} and V^{3p46} (not shown). *C*, G^{4p51} is involved in the hole-into-the-knob contact by its pro-S hydrogen, which is not substituted by the methyl group in the $G^{4p51}A$ mutant. *D*, conserved polar residues in positions *p45* may stabilize the outer pore by forming H-bonds with ascending limbs. In our model the side chain of R^{1p45} interacts with the backbone carbonyl group of N^{1p54}, whereas Q^{3p45} interacts with the backbone NH group of W^{3p52}. These contacts may explain why cysteine substitutions of R^{1p45} and R^{2p45} destabilize binding of the positively charged TTX (27).

(26). This effect can hardly be explained by direct interaction of the TTX molecule with the hydrophobic residue I^{4p46}, which is located in the P-helix and does not protrude in the outer pore. In our model the ascending limbs of all four domains closely approach the same-domain P-helices and tightly pack against them. In particular, the conserved isoleucine I^{4p46} forms a knob-into-the-hole contact with the exceptionally conserved glycine G^{4p51} (Fig. 3, *A* and *B*). Mutation $I^{4p46}V$ creates a void of a methyl group size in the tight intra-repeat contact between the P-helix and the ascending limb. P-helices in our models are practically immobile due to several strong contacts with S6 and S5 helices (15). To fill the void, glycine G^{4p51} would move toward valine V^{4p46} and pull the ascending limb of repeat IV away from the pore axis. The shifted ascending limb would widen the outer pore and thus deform the TTX receptor.

In the Brenton populations of garter snakes, which are about two times less sensitive to TTX than the Warrenton population, the sodium channel has two mutations in the P-loop region: $I^{4p46}V$ and $G^{4p51}A$ (26). At first glance, the methyl group of A^{4p51} would fill the void at the V^{4p46} side chain without causing any shift of the ascending limb of repeat IV. However, closer inspection of our model shows that G^{4p51} is involved in a hole-into-the-knob contact by its pro-S hydrogen, whereas it is the pro-R hydrogen that is substituted by the methyl group in the $G^{4p51}A$ mutant (Fig. 3*C*). In our model, the pro-R hydrogen approaches the ascending limb of domain III suggesting that mutations $G^{4p51}A$ and $I^{4p46}V$ concertedly cause the outer-pore widening, which decreases the TTX sensitivity of the Brenton populations of garter snakes.

The lowest sensitivity to TTX is observed in the Willow-Creek population of garter snakes, whose NaV1.4 channels, besides the above-described mutation $L^{4p46}V$, have three additional mutations in the P-loop region. These include mutation $D^{4p53}N$, which changes a residue that directly interacts with TTX (Fig. 2*A*). Thus, our model explains the intriguing data on the TTX resistance of garter snakes by the influence of mutations $I^{4p46}V$ and $G^{4p51}A$ on the outer-pore geometry and by direct influence of mutation $D^{4p53}N$ on TTX binding.

Other TTX-sensing residues in the P-helix, which do not directly interact with the TTX molecule in our model, can also affect TTX binding by modifying the outer-pore structure. Indeed, the bundle of four ascending limbs contains intrinsically flexible strands, which are not stabilized by H-bonds of a regular secondary structure. Therefore, the geometry of the bundle should be stabilized by specific contacts. Mutations, which affect such stabilizing contacts, would affect the outer-pore structure and therefore the TTX sensitivity of the channel. Intriguingly, cysteine substitutions of highly conserved R^{1p45} and exceptionally conserved R^{2p45} decrease the sensitivity of NaV1.4 to TTX by ~10- and ~1000-fold, respectively (27). These data seem paradoxical because the cationic TTX molecule should electrostatically repel from the cationic arginines and their replacement by cysteines is expected to eliminate the repulsion and hence increase the TTX potency. The fact that the TTX potency is decreased can be explained as follows. In the KcsA K^+ channel, position *p45* is occupied by the glutamate residue whose side chain projects toward the extracellular space, parallel to the ascending limb (supplemental Fig. S2). These data prompt us to suggest that mutations $R^{1p45}C$ and $R^{2p45}C$ eliminate contributions of the arginines in the outer-pore stability and thus affect TTX binding indirectly. Intensive MC-minimizations of our current model from multiple starting orientations of the R^{1p45} and R^{2p45} side chains yielded low-energy conformations in which these side chains donate intra-repeat H-bonds to the backbone carbonyls in positions *p53* (Fig. 3*D*). Noteworthy, positions *1p53* and *2p53* are occupied by TTX-sensing glutamates from the outer-carboxylates ring. In view of our model, the cysteine substitution of R^{1p45} and R^{2p45} would deform the structure of the outer-carboxylate ring and thus its interactions with TTX. The exceptionally conserved Q^{3p45} in the homologous position can also form specific intra-repeat contacts with the ascending-limb backbone of repeat III. Glutamine Q^{4p45} is moderately conserved (67.4.5%), but 28.4% of the sequences contain glutamate E^{4p45}, which can also be en-

gaged in an intra-repeat H-bond with the ascending limb backbone. One such possibility is shown in Fig. 3*D* where the side chain carbonyl of Q^{3p45} accepts an H-bond from the backbone NH group of W^{3p52}. It should be noted however that mutations $Q^{4p45}C$ and $Q^{3p45}C$ have only a small effect on the TTX potency (27). Other specific interactions involving side chains of long H-bonding residues in positions *p45* are also possible.

Na^+ Binding Sites—Previously we used our TTX-based model of the sodium channel (5) to predict putative binding sites for Na^+ ions and propose a scheme of ion permeation. The scheme involves six Na^+ ions: four in the outer-carboxylates ring, one in the selectivity filter ring, and one between the two rings (9). To explore whether this scheme is consistent with our present model, we loaded the outer pore with six Na^+ ions as proposed before (9). The first ion was constrained to D^{3p54}, the second ion between D^{3p54} and D^{4p53}, the third ion between D^{4p53} and E^{1p53}, the fourth ion between E^{1p53} and E^{2p53}, the fifth ion between E^{2p53} and E^{2p50}, and the sixth ion to D^{1p50}. The selectivity-filter lysine K^{3p50} was constrained between E^{2p50} and D^{1p50}. MC-minimization yielded a structure (Fig. 4*A*) in which four Na^+ ions were engaged in cation-π contacts with the conserved tryptophans. The scheme of the Na^+ binding sites is shown in Fig. 4*E*.

The first Na^+ ion in the most extracellular position interacts with D^{3p54}. This ion would not move deeper into the outer pore along the pore axis due to unfavorable interactions with the hydrophobic corner (Fig. 4*B*). The latter is formed by the highly conserved I^{2p52} and hydrophobically conserved residues in position *3p53* where Met, Ile, Thr, and Leu residues are found, respectively, in 78.0, 15.1, 5.0, and 1.8% of the sequences. The second, third, and fourth Na^+ ions are engaged in cation-π interactions with tryptophans W^{3p52}, W^{4p52}, and W^{1p52}, respectively. The fifth Na^+ ion is engaged in cation-π interactions with W^{2p51} below the hydrophobic corner and this ion simultaneously interacts with the outer carboxylate E^{2p53} and the selectivity-filter glutamate E^{2p50}. Importantly, the exceptionally conserved W^{2p51} is located deeper in the outer pore than tryptophans in positions *p52*. According to our model, W^{2p51} would stabilize the Na^+ ion moving from the outer-carboxylates to the selectivity filter. The sixth Na^+ ion is coordinated at the selectivity filter. Our model implies that Na^+ ions move through the outer pore not linearly, but along a spiral path, consecutively occupying positions 1 through 6.

The space between Na^+ ions in our model at the level of the conserved tryptophans is filled with water molecules. Asymmetry of the pore at this level (three tryptophans and the hydrophobic corner) dictates such orientation of the water dipoles, in which partial positive charges are directed toward the hydrophobic corner. Fig. 4, *C* and *D* show models with four and two water molecules at the level of the conserved tryptophans. The water molecules are linked to each other by H-bonds and a water molecule forms H-bonds with M^{3p53}. It should be noted that structures in Fig. 4, *C* and *D* are just possible examples of Na^+ hydration in the outer pore.

Thus, our current model agrees with our previous models in terms of TTX (5) and ion binding (9), but it proposes a new

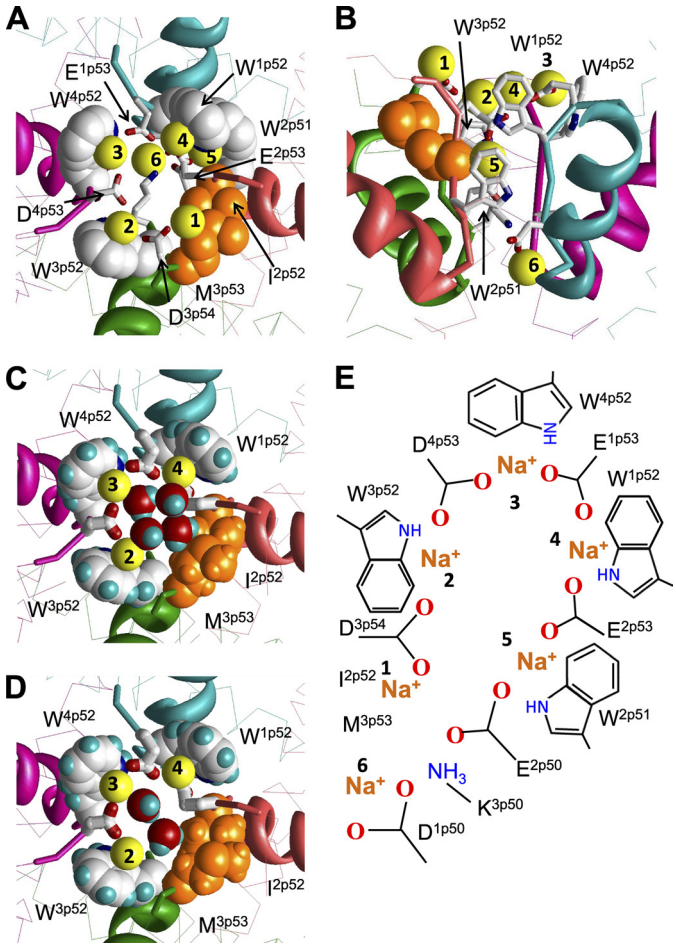

FIGURE 4. **Homology model of the NaV1.4 channel illustrating possible role of conserved tryptophans in ion permeation.** *A* and *B*, extracellular and side views. The side chains of W^{1p52}, W^{3p52}, and W^{4p52} (space-filled with *white carbons* and *blue nitrogens*) along with I^{2p52} and M^{3p53} (space-filled side chains with *orange* heavy atoms) form a ring between the outer carboxylates (*sticks*) and the selectivity filter DEKA locus (*sticks*). Na^+ ions are numbered as in scheme *E*. Ions 1 to 5 interact with the outer carboxylates (9) and ions 2 to 4 are simultaneously engaged in cation-π interactions with the conserved tryptophans in positions *p52*. Exceptionally conserved W^{2p51} provides a cation-attractive transient site between the outer carboxylates and the selectivity filter. A Na^+ ion bound to W^{2p51} can simultaneously interact with an outer carboxylate E^{2p53} and an acidic residue in the DEKA locus (9). *C* and *D*, extracellular views show four and two water molecules, respectively, which fill the gap between Na^+ ions at the level of the conserved tryptophans, providing additional coordination bonds for the first solvation shell of these ions. *E*, scheme of Na^+ binding sites in the outer pore of the Na^+ channel.

structural role for the exceptionally conserved tryptophans, whose π-electrons are predicted to face the ion permeation pathway and thus participate in ion permeation. The structures obtained by MC-minimizing the P-loops domain with TTX on one hand and with Na^+ ions on the other hand are very similar (Fig. 2*D*). The root mean square deviation the ascending-limbs backbone atoms (positions *p50–p54*) between the two structures is as small as 0.4 Å. Na^+ ions, which interact with the conserved tryptophans, are close to the positions of the hydroxyl hydrogens of a bound TTX molecule.

The Outer-pore Model for Ca^{2+} Channels—Modeling the outer pore of calcium channels is challenging due to deficiency of experimental data on binding specific toxins as small as TTX. Recently we developed a model of Ca^{2+} bind-

ing in the calcium channel selectivity filter, which predicts multiple Ca^{2+} chelation patterns involving long flexible side chains in the EEEE ring (6). Our present model of the sodium channel suggests the importance of the inter-repeat H-bonds involving conserved tryptophans for outer-pore stability and ion permeation. Sodium channels evolved from calcium channels (16). Many P-loop residues in sodium channels, including selectivity-filter residues, have changed during the evolution, but tryptophans W^{1p52}, W^{3p52}, and W^{4p52}, did not change. The calcium channel tryptophan, W^{2p52} did not disappear during the evolution, but apparently shifted one position in the N-terminal direction to become exceptionally conserved W^{2p51} (Fig. 1*B*). These data allow us to suggest that the exceptionally conserved tryptophans in calcium channels play roles similar to those that we proposed for sodium channels.

To model the tryptophan ring in the calcium channel, we used distance constraints to impose inter-repeat H-bonds involving the side chains and backbone carbonyls of the four W^{p52}s, MC-minimized the structure, and arrived at the model shown in Fig. 5. How could Ca^{2+} ions permeate through the tryptophan ring? Unlike Na^+ ions, which can be directly engaged in cation-π interactions with tryptophans, strongly hydrated Ca^{2+} ions should interact with the aromatic moieties through water molecules (28). We placed a Ca^{2+} ion with four waters in the W^{p52} ring, constrained D^{2p51} and E^{2p53} to the ion as proposed before (6), MC-minimized the structure with the constraints, and refined it without constraints. In the resulting structure (Fig. 5, *B* and *C*) four waters and the Ca^{2+} ion are in the same plane. The hydrated Ca^{2+} fits perfectly in the tryptophan ring. Each water molecule interacts with the tryptophan π-electrons by a hydrogen atom. The inner "diameter" of the H-bonded W^{p52} ring is model-independent. The perfect match of the inner diameter with the outer "diameter" of the Ca^{2+} ion surrounded by four waters is hardly a coincidence. The Ca^{2+} ion in the tryptophan ring is hexacoordinated (four waters, E^{2p53}, and D^{2p51}) and occupies the center of the octahedral bipyramid. This coordination geometry is found for calcium in many x-ray structures (29) and is predicted to be the most populated in water (30).

Combining the current outer-pore model with our recent modeling study of Ca^{2+} binding to the selectivity-filter glutamates (6), we propose the following permeation scheme (Fig. 5, *A* and *D*). It involves two Ca^{2+} ions bound to the selectivity filter glutamates, a Ca^{2+} ion at the level of tryptophan ring and a Ca^{2+} ion bound to the outer ring of residues in positions *p54*. The outer carboxylates are not conserved in calcium channels (Fig. 1). In some channels the outer carboxylates may attract Ca^{2+} ions from the extracellular media to the outer pore. Positions *p54* are occupied by residues whose side chains contain at least one electronegative atom (99.0, 41.1, 77.3, and 97.9% in repeats I, II, III, and IV, respectively). These residues would contribute to the first solvation shell of the incoming Ca^{2+} ion. The incoming Ca^{2+} ion would exchange its waters to the water molecules in the tryptophan ring, which along with the highly conserved D^{2p51} would coordinate the ion. Vacancies in the first coordination spheres of other Ca^{2+} ions would be also filled by waters (6). Thus, our model suggests that the tryptophan ring participates in

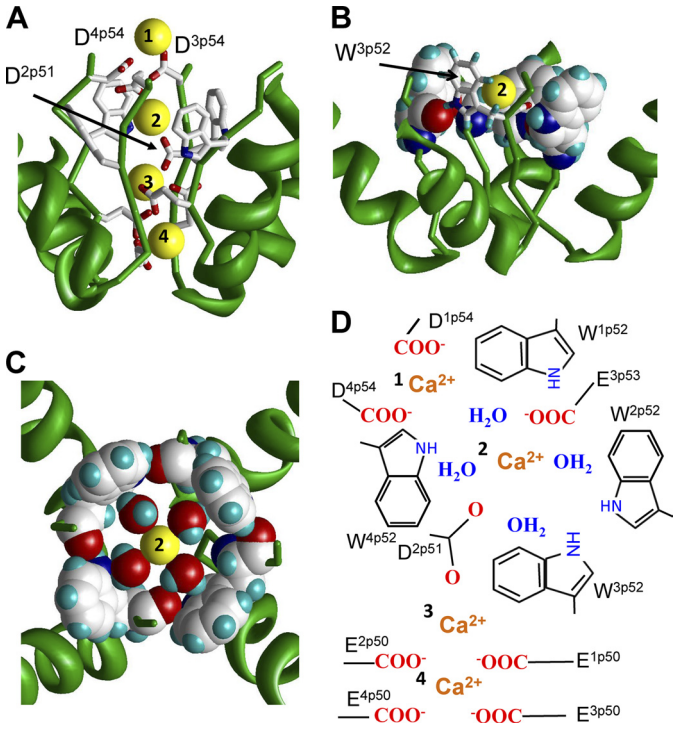

FIGURE 5. **Possible role of exceptionally conserved tryptophans in positions *p52* of calcium channels.** *A*, side view of the predicted pattern of Ca^{2+} binding in the CaV1.2 model. The most extracellular Ca^{2+} ion is coordinated by the outer carboxylates D^{1p54} and D^{4p54}. The outer carboxylate E^{3p53} and highly conserved D^{2p51} coordinate the hydrated Ca^{2+} ion in the W^{p52} ring. Two Ca^{2+} ions at lower levels of the outer pore are coordinated by the selectivity filter glutamates. *B*, side view at a Ca^{2+} ion in the ring of W^{52}s. Residues W^{1p52}, W^{2p52}, and W^{4p52} are *space-filled*, and W^{3p52} is shown by *sticks*. *C*, top view at ring of four W^{p52}s, which is stabilized by inter-repeat H-bonds. Each H-bond involves the side chain NH group in the given repeat and the backbone carbonyl in the next repeat. In this arrangement, the tryptophan side chains form a cation-attractive path by maximizing exposure of π-electrons to the pore lumen. The size of the tryptophan-ring inner surface matches the dimension of the Ca^{2+} ion with the first hydration shell. Four water molecules and the Ca^{2+} ion lie in a plane, which is normal to the pore axis. D^{3p54} and highly conserved D^{2p51} provide two axial coordination bonds (not shown) to complete the hexa-coordinated geometry, which is seen in x-ray structures and predicted by molecular dynamics simulations (see text). The water oxygens interact with the Ca^{2+} ion, while water hydrogens interact with π-electrons of the tryptophans. *D*, schematic view of model *A*. Calcium ions are labeled with numbers.

the permeation process by stabilizing the conducting conformation of the outer pore and by helping to deliver the external Ca^{2+} ion to the selectivity filter. The water molecules may not move with Ca^{2+} and remain H-bonded to π-electrons of the tryptophans, suggesting a mechanism of Ca^{2+} dehydration.

Comparing Calcium Binding in the Selectivity Filters of Ca^{2+} and Na^+ Channels—The selectivity filter region in the Ca^{2+} channel has a net charge of -5 proton charge units (the EEEE locus and D^{2p51}), while this region in the Na^+ channel has only -1 proton charge units (the DEKA locus and neutral W^{2p51}). Na^+ channels are blocked by divalent cations at the selectivity filter level (28). To reveal possible structural determinants of the block, we docked a Ca^{2+} ion into the outer-pore region of the Na^+ channel from multiple starting positions and MC-minimized the complex using an approach described elsewhere (31). In the energetically optimal structures, the Ca^{2+} ion strongly bound to D^{1p50} and E^{2p50} in the

DEKA locus and destroyed contacts of these residues with the ammonium group of K^{3p50} that moved toward the inner pore (Fig. 2*E*). In some of the MC-minimized structures, the Ca^{2+} ion bound to the outer carboxylates without destroying the salt bridge between D^{1p50} and K^{3p50}. The conserved tryptophans W^{1p52}, W^{3p52}, and W^{4p52}, which are located externally to the selectivity filter, were too far from the Ca^{2+} ion bound to the DEKA locus. However, the aromatic ring of Y^{1p51}, which is 4–5 Å from the Ca^{2+} ion in our model, would interact with the ion through a water molecule in agreement with the proposition that interaction of Y^{1p51} and the channel-blocking Ca^{2+} ion is mediated by a water molecule (28). The proximity of Y^{1p51} to the Ca^{2+} ion is supported by the data that NaV1.5, which contains C^{1p51}, is less sensitive to the Ca^{2+} block than NaV1.4 (32). The conserved W^{2p51} is at a similar distance from the Ca^{2+} ion and could also interact with it through a water molecule.

In the Ca^{2+} channel, up to five negative charges at the selectivity filter allow simultaneous binding of two or three calcium ions (6). The repulsion between the ions weakens the binding and facilitates the ion permeation (6). In the sodium channel, binding of the Ca^{2+} ion to D^{1p50} and E^{2p50} is very strong because no additional binding sites for a divalent cation are within 6 Å from the DEKA locus. The lack of neighboring divalent cations likely explains why Ca^{2+} ions do not permeate through the sodium channel, but block it.

DISCUSSION

In the present work we aligned many sequences of the P-loop segments of sodium and calcium channels and revealed exceptionally and highly conserved residues whose roles were not explained before. We suggest that the evolutionary conservation of these residues is due to their participation in maintaining the outer-pore structure and their involvement in the ion permeation. Our models provide a structural explanation for the conservation of the residues and relate it to functional peculiarities of calcium and sodium channels. The proposed tryptophan ring is symmetrical in calcium channels. A single Ca^{2+} ion surrounded by four water molecules fits snugly into the ring. The conserved D^{2p51} would deliver the ion to the selectivity-filter glutamates. The selectivity-filter glutamates along with D^{2p51} may bind three Ca^{2+} ions (6). A system of three divalent ions and five ionized carboxylates has an excessive positive charge of one proton-charge unit that may facilitate the ion permeation (6). In sodium channels, the positive charge of one proton-charge unit in the fully ionized DEKA ring is counterbalanced by a Na^+ ion. If aspartate D^{2p51}, which is present in all Ca^{2+} channels, were to remain in Na^+ channels to deliver a monovalent cation to the DEKA ring, the net negative charge of the amino acids at the selectivity filter (−2 proton charge units) would attract a Ca^+ ion and thus decrease the channel selectivity to Na^+. Evolution of Na^+ channels from Ca^{2+} channels involved substitution of the negatively charged aspartate D^{2p51} with the electroneutral (but cationophilic) W^{2p51}. The substitution, which may have resulted from deletion of D^{2p51} in the Ca^{2+} channel sequence, likely helped to reduce affinity for Ca^{2+} ions.

The exact role of residues in position *2p51* needs further experimental analysis. It is well known that mutations in the EEEE locus in calcium channels and the DEKA locus in sodium channels, which did not change residues in position *2p51,* alter the Na^+ and Ca^{2+} selectivity (33, 34). On the other hand, the observation that the prokaryotic homotetrameric channel NaChBac has the EEEE locus initially led to categorize it as a Ca^{2+}-selective channel (8). Subsequently expressed NaChBac is found to be a Na^+-selective channel (35). Additional acidic residues in the ascending limbs, in particular in position *p51*, are required to render the NaChBac channel Ca^{2+}-selective (36).

Here we proposed that the exceptionally conserved tryptophans in the ascending limbs of calcium and sodium channels participate in stabilizing the outer-pore structure by H-bonds, which involve the side chain NH groups. The ascending limbs contain free backbone carbonyls, which can accept H-bonds. In our model of CaV1.2, the side chain of W^{p52} in a given repeat donates an H-bond to the backbone carbonyl of the neighboring-repeat W^{p52} (Fig. 5). A similar network of H-bonds involving tryptophans W^{p52} is proposed for the sodium channels. Importantly, the tryptophan rings do not preclude the selectivity filter and outer carboxylates residues from exposing their side chains into the pore lumen and thus participate in the ion permeation process. Due to the network of inter-repeat H-bonds, the outer-pore lumen at the level of p52 is rather narrow, but in our model it still accommodates a TTX molecule. It will be interesting to further explore whether our narrow outer-pore model is consistent with intriguing data on synergistic and antagonistic interactions between tetrodotoxin and mu-conotoxin in blocking voltage-gated sodium channels (37).

Although Ca^{2+} and Na^+ channels are believed to have similar architecture of the outer pore, the ion permeation mechanisms in these channels are significantly different. Thus, strong ion coupling in the Ca^{2+} channels seems critical for the anomalous mole fraction effect, while the narrow part of the Na^+ channel pore is predominantly single-occupied (16). Our computational methodology does not allow a direct detailed simulation of the flux coupling. However, our models predict that the equilibrium binding sites for permeating ions are separated by 5–6 Å along the pore axis. At such distances, the divalent ions in the Ca^{2+} channel repel each other more strongly than monovalent ions in the Na^+ channel. This repulsion compensates the strong binding of divalent ions to their binding sites.

Limitations of our model should be spelled out. Our computational methodology allows one to reproduce structural details of known complexes of proteins with organic ligands (38) and calcium ions (31). However a homology model, which includes only a part of a large transmembrane protein and lacks membrane lipids, is not expected to correspond to the global energy minimum. Therefore, we initially preserved the structural stability of the models by pin constraints imposed to alpha carbons of the P-helices (general folding) and specific H-bonding constrains involving conserved tryptophans and polar residues in positions *p45*. When metal ions and **a** TTX molecule (in Na^+ channel) were added, the mod-

els did not change significantly even after intensive MC-minimizations without constraints because permeating cations counterbalanced excessive negative charges of the pore-exposed residues, while TTX stabilized the model by H-bonds and other interactions. (The importance of permeating cations for supporting the native structure of ion channels is well known.) Thus, our modeling approach allowed us to propose specific contacts, which stabilize the ascending limbs in sodium and calcium channels. Imposing these contacts as constraints in MC minimizations resulted in the models that can explain various experimental data.

Another limitation is related to the proposed permeation mechanism. We did not model the permeation process, but predicted transient binding sites for permeant ions. Therefore, the proposed details of the permeation mechanisms should be considered as hypotheses derived from static snapshots. The MCM method used in the present work is not appropriate for realistic modeling of the permeation process because it involves large random transitions between sampled structures. The intensive sampling of the conformational space allows predicting stable structures, but MCM neglects local energy barriers, which are important to simulate the ion permeation. The proposed details of the ion permeation mechanism could be tested by computing the free energy profile for the ion permeating through the outer pore, but such simulations, which would require different computational methodologies, are beyond the scope of our study. Our models lay the groundwork for the dynamic calculations that will be needed to address specific effects such as ion coupling in the pore.

The outer pore of ion channels governs selectivity, permeation, slow inactivation, and binding of toxins. Many data indicate similar dispositions of S6, S5, and P-helices in voltage-gated potassium, calcium, and sodium channels. However, the ascending limbs in calcium and sodium channels are generally believed to fold not like in potassium channels. Here we elaborated our previous models (5, 6) to explain roles of exceptionally conserved residues, which were revealed in multiple-sequence alignments, and explained recently published experimental data. The fact that the P-helices and S6s in our homology models are built using a potassium channel template further supports the notion that the folding of these segments in potassium, sodium, and calcium channels is generally similar.

Acknowledgments—We thank Ludmila Milova for generating multiple sequence alignments and preparing Fig. 1. We thank Daniel Garden for reading the manuscript. Computations were made possible by the facilities of the Shared Hierarchical Academic Research Computing Network.

REFERENCES

1. Dudley, S. C., Jr., Chang, N., Hall, J., Lipkind, G., Fozzard, H. A., and French, R. J. (2000) *J. Gen. Physiol.* **116,** 679–690
2. Bruhova, I., and Zhorov, B. S. (2010) *J. Gen. Physiol.* **135,** 261–274
3. Zhorov, B. S., and Tikhonov, D. B. (2004) *J. Neurochem.* **88,** 782–799
4. Lipkind, G. M., and Fozzard, H. A. (1994) *Biophys. J.* **66,** 1–13
5. Tikhonov, D. B., and Zhorov, B. S. (2005) *Biophys. J.* **88,** 184–197
6. Cheng, R. C., Tikhonov, D. B., and Zhorov, B. S. (2010) *Eur. Biophys J.* **39,** 839–853
7. Zhorov, B. S., Folkman, E. V., and Ananthanarayanan, V. S. (2001) *Arch. Biochem. Biophys.* **393,** 22–41
8. Durell, S. R., and Guy, H. R. (2001) *Biochem. Biophys. Res. Commun.* **281,** 741–746
9. Tikhonov, D. B., and Zhorov, B. S. (2007) *Biophys. J.* **93,** 1557–1570
10. Weiner, S. J., Kollman, P. A., Case, D. A., Singh, U. C., Ghio, C., Alagona, G., Profeta, S., and Weiner, P. (1984) *J. Am. Chem. Soc.* **106,** 765–784
11. Weiner, S. J., Kollman, P. A., Nguyen, D. T., and Case, D. A. (1986) *J. Comput. Chem.* **7,** 230–252
12. Lazaridis, T., and Karplus, M. (1999) *Proteins* **35,** 133–152
13. Dewar, M. J., Zoebisch, E. G., Healy, E. F., and Stewart, J. J. (1985) *J. Amer. Chem. Soc.* **107,** 3902–3909
14. Li, Z., and Scheraga, H. A. (1987) *Proc. Natl. Acad. Sci. U. S. A.* **84,** 6611–6615
15. Bruhova, I., Tikhonov, D. B., and Zhorov, B. S. (2008) *Mol. Pharmacol.* **74,** 1033–1045
16. Hille, B. (2001) *Ion Channels of Excitable Membranes*, Sinauer Associates Inc., Sunderland, MA
17. Struyk, A. F., and Cannon, S. C. (2002) *J. Gen. Physiol.* **120,** 509–516
18. Xiong, W., Li, R. A., Tian, Y., and Tomaselli, G. F. (2003) *J. Gen. Physiol.* **122,** 323–332
19. Tsushima, R. G., Li, R. A., and Backx, P. H. (1997) *J. Gen. Physiol.* **109,** 463–475
20. Tsang, S. Y., Tsushima, R. G., Tomaselli, G. F., Li, R. A., and Backx, P. H. (2005) *Mol. Pharmacol.* **67,** 424–434
21. Carbonneau, E., Vijayaragavan, K., and Chahine, M. (2002) *Pflugers Arch.* **445,** 18–24
22. Santarelli, V. P., Eastwood, A. L., Dougherty, D. A., Horn, R., and Ahern, C. A. (2007) *J. Biol. Chem.* **282,** 8044–8051
23. Chen, L. Q., Chahine, M., Kallen, R. G., Barchi, R. L., and Horn, R. (1992) *FEBS Letts.* **309,** 253–257
24. Backx, P. H., Yue, D. T., Lawrence, J. H., Marban, E., and Tomaselli, G. F. (1992) *Science* **257,** 248–251
25. Satin, J., Kyle, J. W., Chen, M., Bell, P., Cribbs, L. L., Fozzard, H. A., and Rogart, R. B. (1992) *Science* **256,** 1202–1205
26. Geffeney, S. L., Fujimoto, E., Brodie, E. D., 3rd, Brodie, E. D., Jr., and Ruben, P. C. (2005) *Nature* **434,** 759–763
27. Yamagishi, T., Li, R. A., Hsu, K., Marbán, E., and Tomaselli, G. F. (2001) *J. Gen. Physiol.* **118,** 171–182
28. Santarelli, V. P., Eastwood, A. L., Dougherty, D. A., Ahern, C. A., and Horn, R. (2007) *Biophys. J.* **93,** 2341–2349
29. McPhalen, C. A., Strynadka, N. C., and James, M. N. (1991) *Adv. Protein Chem.* **42,** 77–144
30. Ikeda, T., Boero, M., and Terakura, K. (2007) *J. Chem. Physics* **127,** 074503-1–074503-8
31. Cheng, R. C., and Zhorov, B. S. (2010) *Eur. Biophys. J.* **39,** 825–838
32. Chahine, M., Chen, L. Q., Kallen, R. G., Barchi, R. L., and Horn, R. (1992) *Biophys. J.* **62,** 37–40
33. Heinemann, S. H., Terlau, H., Stühmer, W., Imoto, K., and Numa, S. (1992) *Nature* **356,** 441–443
34. Tang, S., Mikala, G., Bahinski, A., Yatani, A., Varadi, G., and Schwartz, A. (1993) *J. Biol. Chem.* **268,** 13026–13029
35. Ren, D., Navarro, B., Xu, H., Yue, L., Shi, Q., and Clapham, D. E. (2001) *Science* **294,** 2372–2375
36. Yue, L., Navarro, B., Ren, D., Ramos, A., and Clapham, D. E. (2002) *J. Gen. Physiol.* **120,** 845–853
37. Zhang, M. M., McArthur, J. R., Azam, L., Bulaj, G., Olivera, B. M., French, R. J., and Yoshikami, D. (2009) *Channels* **3,** 32–38
38. Garden, D. P., and Zhorov, B. S. (2010) *J. Computer-aided Mol. Design* **24,** 91–105